

Loading and Releasing Behavior of Selenium and Doxorubicin Hydrochloride in Hydroxyapatite with Different Morphologies

Jing Gao, Jinhui Huang, Rui Shi, Jiawei Wei, Xiaoyu Lei, Yichen Dou, Yubao Li, Yi Zuo,* and Jidong Li*

Cite This: *ACS Omega* 2021, 6, 8365–8375

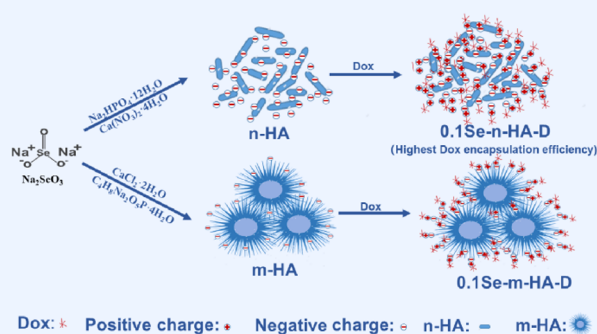
Read Online

ACCESS |

Metrics & More

Article Recommendations

ABSTRACT: Doxorubicin (Dox)-loaded or selenium-substituted hydroxyapatite (HA) has been developed to achieve anti-osteosarcoma or bone regeneration in a number of studies. However, currently, there is a lack of studies on the combination of Dox and selenium loading in/on HA and comparative research studies on which form and size of HA are more suitable for drug loading and release in the treatment osteogenesis after osteosarcoma resection. Herein, selenium-doped rod-shaped nano-HA (n-HA) and spherical mesoporous HA (m-HA) were successfully prepared. The doping efficiency of selenium and the Dox loading capacity of selenium-doped HA with different morphologies were studied. The release kinetics of Dox and the selenium element in phosphate-buffered saline with different pH values was also comparatively investigated. The drug loading results showed that n-HA exhibited 3 times higher selenium doping amount than m-HA, and the Dox entrapment efficiency of selenium-doped n-HA (0.1Se-n-HA) presented 20% higher than that of selenium-doped m-HA (0.1Se-m-HA). The Dox release behaviors of HA in two different morphologies showed similar release kinetics, with almost the same Dox releasing ratio but slightly more Dox releasing amount in selenium-doped HA than in HA without selenium. The selenium release from selenium-doped n-HA-D (0.1Se-n-HA-D) particles was 2 times as much as that of selenium-doped m-HA-D (0.1Se-m-HA) particles. Our study indicated that n-HA loaded with Dox and selenium may be a promising drug delivery strategy for inhibition of osteosarcoma recurrence and promoting osteogenesis simultaneously.



1. INTRODUCTION

Osteosarcoma is the most common malignant bone tumor in children and adolescents.^{1,2} It has a strong invasive force, the 5-year survival rate is about 50–75%,³ and the amputation rate is as high as 10%, which seriously endangers human health. Studies have shown that the main factors affecting the recurrence of osteosarcoma are surgical margins and chemotherapy, and positive surgical resection margins will lead to cancer cells residual to tumor recurrence; however, some osteosarcomas cannot be resected extensively due to the anatomical location, which greatly increases the risk of recurrence.⁴ In order to prevent tumor recurrence, preoperative and postoperative chemotherapy can be used as auxiliary ways to reduce the risk of recurrence.⁵

Doxorubicin (Dox), an anthracycline drug with a broad anticancer spectrum, is one of the reliable conventional chemotherapy drugs and can be used in the treatment of osteosarcoma.⁶ However, the multidrug resistance of osteosarcoma greatly reduces the drug curative effect.^{7,8} Some reports introduced that selenite can bring down the drug resistance of the tumor and reduce the side effects of anticancer drugs for protecting normal tissues.⁹ In addition, many studies have proved that selenite also has a certain role in

the curing osteosarcoma¹⁰ and inhibition of tumor metastasis.¹¹ Wang et al. reported that selenium doping hydroxyapatite (HA) can promote apoptosis of osteosarcoma cells (MG-63 cells) through selenium activating the intrinsic mitochondrial apoptotic pathway.¹² In addition, a porous silica–folic acid–copper sulfide nanocomposite with a combined loading of selenium and Dox showed good efficiency to inhibit cancer cell proliferation.¹³ Therefore, combining Dox and sodium selenite as an anticancer drug is a promising way for anti-osteosarcoma.¹⁴

On account of the side effects of chemotherapy drugs, drug dosage is greatly restricted and unable to get the best antitumor effect;¹⁵ therefore, the local use of anticancer drugs can improve the local drug concentration and reduce systemic side effects; for example, Zheng et al. used pH-

Received: January 6, 2021

Accepted: March 5, 2021

Published: March 16, 2021



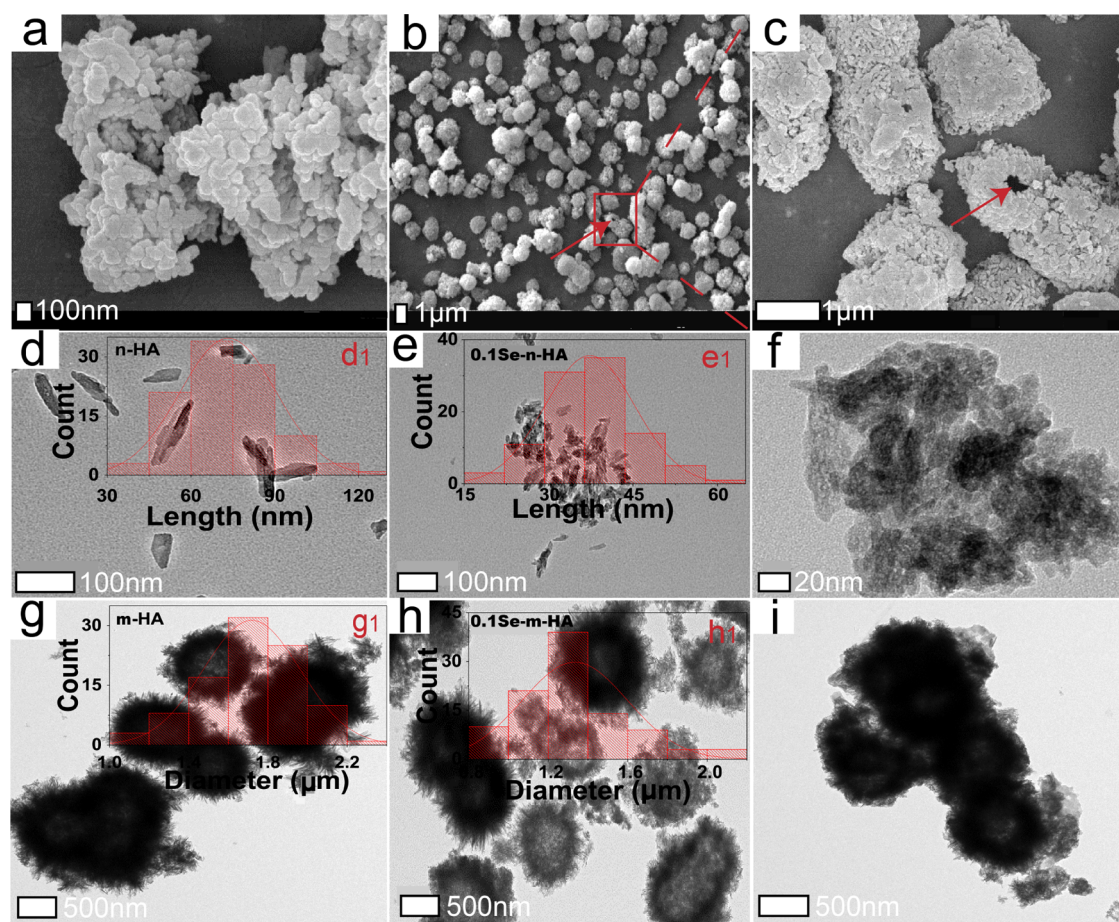


Figure 1. SEM images of n-HA (a) and m-HA (b,c); TEM micrographs of n-HA (d), 0.1Se-n-HA (e), 0.1Se-n-HA-D (f), m-HA (g), 0.1Se-m-HA (h), and 0.1Se-m-HA-D (i); particle size distribution of n-HA (d₁), 0.1Se-n-HA (e₁), m-HA (g₁), and 0.1Se-m-HA (h₁). The red arrows in (b,c) point to the hollow structure of m-HA.

responsive polyion complex micelles,¹⁶ and Zhang et al. used tumor microenvironment-responsive hyaluronate–calcium carbonate hybrid nanoparticles¹⁷ to control Dox intracellular delivery and upregulated antitumor efficacy and reduced side effects. Meanwhile, the explosive release of anticancer drugs is contraindicated. In order to achieve long-term effective release of drugs, carrier materials with good biocompatibility and which enable sustained release of drugs are needed.¹⁸

In recent years, nano-HA and micro-HA have been widely used as drug delivery carriers because their large specific surface area and surface charge enable them to load drugs;^{12,19,20} especially, these nanomedicines with prolonged drug circulation and reduced drug toxicity are considered a superior treatment option for cancer.^{21,22} Although HA is too brittle to maintain bone strength, its good biocompatibility and drug carrier ability make it significant to composite with other polymers to achieve good mechanical properties,²³ and the composition and structure of synthetic HA are very similar to those of the natural bone mineral. HA is widely used as a bone substitute and presents excellent bone repair capacity;^{24–26} in addition, HA has been shown to possess anticancer effects.²⁷ HA integrates the triple functions of anticancer, promotion of osteogenesis, and loading drugs; therefore, HA loaded with anticancer drugs may be an ideal choice for preventing tumor recurrence and promoting bone regeneration after osteosarcoma resection. Although studies have been reported on HA loaded with Dox or selenium-doped HA, these studies reported

only a single type of HA loaded with a single drug.^{19,28–31} Single anticancer drugs have limited effectiveness and are often combined with other drugs to synergistically combat cancer, and some studies described Dox or sodium selenite in combination with other drugs.^{32–34} For instance, Zhang et al. developed hyaluronate nanogels for intracellular codelivery of Dox and cisplatin to anti-osteosarcoma.³⁵ However, systematic comparative studies on the simultaneous loading of Dox and selenium on/in HA with different morphologies and their drug release behavior have not yet been reported. In this study, we synthesized rod-like selenium-doped nano-HA (n-HA) and spherical mesoporous selenium-doped HA (m-HA) and studied the doping efficiency of selenium and the Dox loading capacity, hoping to achieve a synergistic anti-osteosarcoma effect. The release kinetics of Dox and the selenium element in phosphate-buffered saline (PBS) with different pH values was also comparatively investigated. Our study intends to provide a potential drug delivery strategy for simultaneous tumor inhibition and osteogenesis promotion after osteosarcoma resection as well as to provide an insight for selecting the ideal morphology of drug carriers.

2. RESULTS AND DISCUSSION

2.1. Morphology of HA. Figure 1 shows the morphology of n-HA, 0.1Se-n-HA, 0.1Se-n-HA-D, m-HA, 0.1Se-m-HA and 0.1Se-m-HA-D, and their particle size distribution. The n-HA, 0.1Se-n-HA, and 0.1Se-n-HA-D particles showed a short rod-

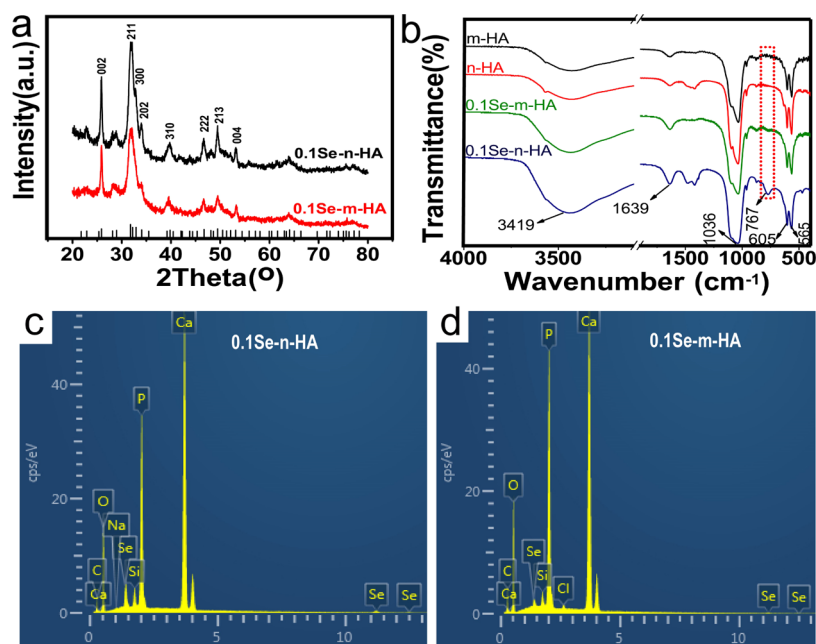


Figure 2. XRD patterns (a) and FTIR spectra (b) of the selenium-doped HA with the molar ratios of Se/P = 0 (n-HA and m-HA) and Se/P = 0.1 (0.1Se-n-HA and 0.1Se-m-HA); EDS spectrum of 0.1Se-n-HA (c) and 0.1Se-m-HA (d).

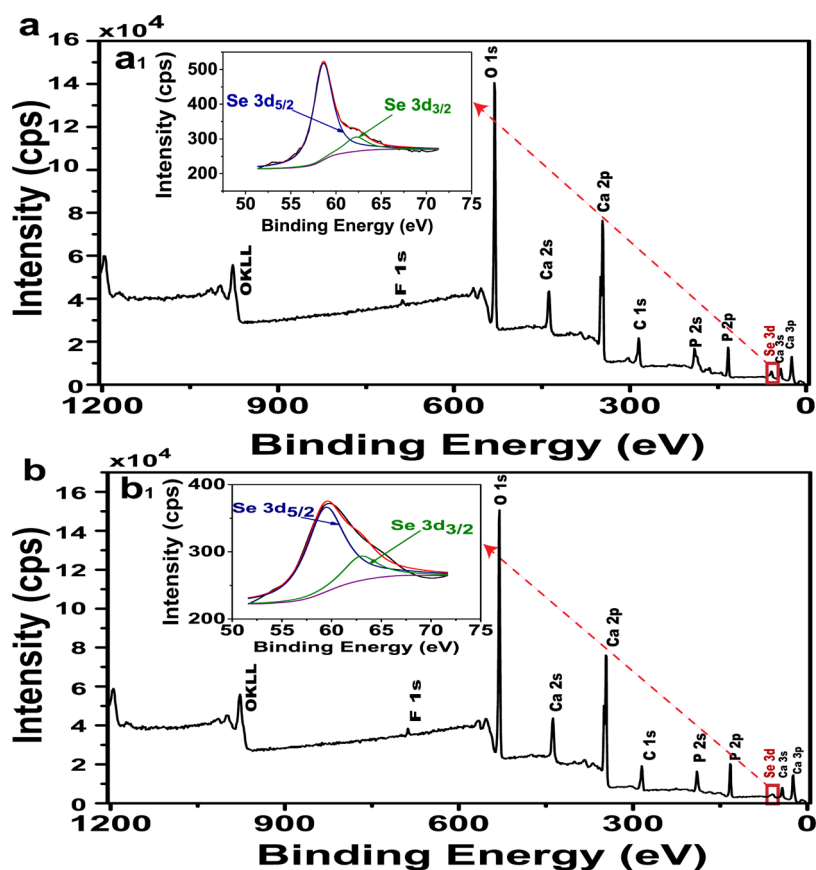


Figure 3. XPS spectrum of 0.1Se-n-HA (a) and 0.1Se-m-HA (b) and the resolution spectra of Se (a₁, b₁), respectively.

like morphology (Figure 1d–f). The length of n-HA was mainly distributed at 60–90 nm (Figure 1d₁), while 0.1Se-n-HA showed a shorter particle length (30–45 nm, Figure 1e₁). The m-HA, 0.1Se-m-HA, and 0.1Se-m-HA-D particles showed a hollow spherical morphology (Figure 1b,c,g-i), and the size

of 0.1Se-m-HA (with a diameter distribution of 1–1.4 μm , Figure 1h₁) was smaller than the size of m-HA (with a diameter distribution of 1.4–2 μm , Figure 1g₁).

The results from scanning electron microscopy (SEM) and transmission electron microscopy (TEM) observation in-

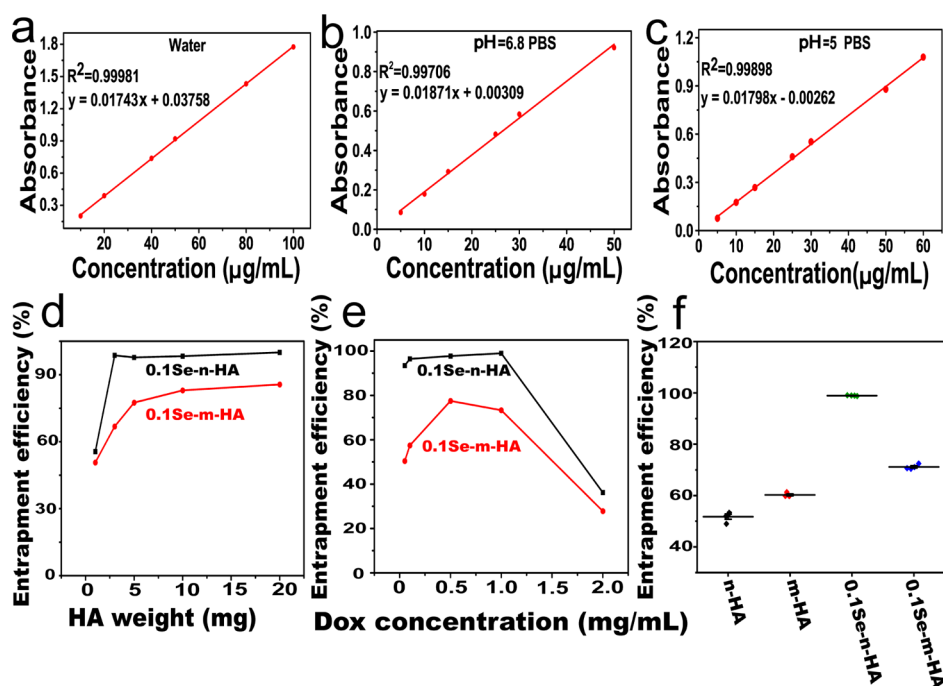


Figure 4. Standard curves of absorbance–Dox concentration in deionized water (a), PBS with a pH of 6.8 (b), and PBS with a pH of 5 (c); encapsulation efficiency with different selenium-doping HA weights when the Dox concentration was kept at 1 mg/mL (d); encapsulation efficiency with different Dox concentrations when the selenium-doping HA weight was kept at 5 mg (e); encapsulation efficiency of different kinds of HA when the weight was fixed at 5 mg and the Dox concentration was fixed at 1 mg/mL (f).

indicated that selenium doping would reduce the crystal size of HA but did not change the shape of HA obviously.³⁶ The reduction of the HA crystal size after selenium doping may be attributed to the fact that the HA crystal lattice is susceptible to ion substitution, and ion exchanging may change the cell unit, the lattice parameters, and the crystallite size. The size of the SeO_3^{2-} ion is similar to the size of the PO_4^{3-} ion, so the substitution of PO_4^{3-} with SeO_3^{2-} is possible. However, difference still exists in the structure and charge of SeO_3^{2-} and PO_4^{3-} ; for instance, SeO_3^{2-} is a flat trigonal pyramid structure with double-charge ions, while PO_4^{3-} is a regular tetrahedron with triple-charge ions; therefore, the substitution of PO_4^{3-} with SeO_3^{2-} may result in some Ca^{2+} and OH^- ions being removed and lattice structure distortion to some extent and eventually reduce the crystal structural integrity and crystal size.³⁷ The TEM images (Figure 1e,f) also indicated that loading of Dox did not change the morphology and size of 0.1Se-n-HA obviously, except leading HA particles to form cluster, and this phenomenon was also found in the 0.1Se-m-HA and 0.1Se-m-HA-D samples (Figure 1h,i). The agglomeration phenomenon of Dox-loaded samples may be attributed to the residual charge on the Dox molecule, which when adsorbed on the HA surface would attract other HA particles until the charge reaches equilibrium.

It should be mentioned that the n-HA particles in Figure 1a are severely agglomerated, which is mainly because the dried powder was directly used for SEM observation, and nanoparticles had a large specific surface area and surface active points, tending to agglomerate in the drying process. Such agglomeration can be avoided by ultrasonic dispersion in ethanol prior to use.

2.2. Composition of Selenium-Doped HA. As shown in Figure 2a, the X-ray diffraction (XRD) patterns of all products exhibited the same characteristic peaks of the typical HA

crystal structure (JCPDS card no. 09-0432). Diffraction peaks at 25.89, 31.89, 32.78, 34.02, 39.64, 46.65, 49.4, and 53.15° assigned to the (002), (211), (300), (202), (310), (222), (213), and (004) planes, respectively,¹¹ indicated that HA can still maintain its original crystal structure when the amount of selenium doping is at the ratio of Se/P = 0.1.

In the Fourier transform infrared (FTIR) spectra (Figure 2b), the peak at 1036 cm^{-1} is ascribed to the P–O antisymmetric stretching vibration (ν_3), the peaks at 605 and 565 cm^{-1} belong to the O–P–O bending mode (ν_4), the peaks at 3419 and 1639 cm^{-1} belong to H_2O , and the peak at 767 cm^{-1} belongs to SeO_3^{2-} .^{38–40} Unsurprisingly, the peaks belonging to PO_4^{3-} and SeO_3^{2-} were found in all selenium-doped HA samples. Notably, the absorption peak intensity of SeO_3^{2-} of 0.1Se-n-HA rod-like crystals was stronger than the peak intensity of 0.1Se-m-HA mesoporous spherical particles, suggesting that the doping efficiency of selenium in rod-like crystals was higher than that in mesoporous spherical particles.

Energy-dispersive spectroscopy (EDS) spectra (Figure 2c,d) and the X-ray photoelectron spectroscopy (XPS) spectrum (Figure 3) further confirmed the presence of the Se element. EDS spectra (Figure 2c,d) showed that the selenium peak in rod-like 0.1Se-n-HA was higher than the selenium peak in spherical 0.1Se-m-HA, which was consistent with the results of FTIR analysis. The Se 3d spectrum peaks at around 59 eV and was interpreted to be the Se(IV) species (NIST),^{41,42} so the presence of Se 3d_{5/2} (the binding energy was about 59 eV) with a much higher peak value than Se 3d_{3/2} (the binding energy was about 62 eV) in the resolution spectrum (Figure 3a₁,b₁) indicated that the valence of selenium in Se-substituted HA was almost +4,^{41,43–45} and the peak intensity of binding energy around 59 eV of 0.1Se-n-HA was higher than that of 0.1Se-m-HA, which also confirmed the higher content of Se in 0.1Se-n-HA than in 0.1Se-m-HA (Figure 3a₁,b₁). Although the

Table 1. BET Surface Area of HA

	n-HA	0.1Se-n-HA	0.1Se-n-HA-D	m-HA	0.1Se-m-HA	0.1Se-m-HA-D
BET (m ² /mg)	25	86	35	80	109	40

Se element was doped in HA, Figure 3a,b confirms that the Ca and P elements were the main elements on the surface of 0.1Se-n-HA and 0.1Se-m-HA.⁴⁶ These results indicated that the selenium element maintains at a +4 valence state after doping into HA and did not change the main components of HA.

In order to determine the accurate selenium content in selenium-doped HA, we detected it by inductively coupled plasma mass spectroscopy (ICP-MS) and X-ray fluorescence (XRF). The results of ICP-MS showed that there were 422 and 115.2 μg of selenium in 10 mg of 0.1Se-n-HA and 10 mg of 0.1Se-m-HA, respectively. The results of XRF were very close to those of ICP-MS, that is, 425.58 and 137.93 μg of selenium in 10 mg of 0.1Se-n-HA and 10 mg of 0.1Se-m-HA, respectively. The actual doping amount of selenium (approximately 422–425 μg) in 10 mg of 0.1Se-n-HA was just slightly lower than the theoretical addition amount of 430 μg . However, the actual doping amount in 10 mg of 0.1Se-m-HA was approximately 110–150 μg , which was only 35% of the theoretical addition amount.

The large difference of selenium doping amount between 0.1Se-n-HA and 0.1Se-m-HA may be attributed to its different synthesized conditions. In aqueous solution, phosphocreatine used as a template for the synthesis of m-HA will break down into phosphoric acid and creatine,⁴⁷ and the guanidine group in the dissociated creatine may bind with some SeO_3^{2-} ions reversibly due to the similar size, charge, and structure of the SeO_3^{2-} ion to the PO_4^{3-} ion.³⁷ The binding between the guanidine group and the SeO_3^{2-} ion will reduce the amount of the dissociative SeO_3^{2-} ion in the solution, which results in less opportunity for SeO_3^{2-} ion entering into the crystal of m-HA, thus reducing the doping amount of the final selenium element in 0.1Se-m-HA.

2.3. Dox Loading. The correlation coefficients (R^2) of standard curves shown in Figure 4a–c were all over 0.99 in deionized water, in PBS with a pH of 6.8 and in PBS with a pH of 5, which indicated the good fitting degree of the standard curves and guaranteed the reliability of detection of the Dox concentration via a UV spectrophotometer. In order to explore the Dox loading efficiency in HA, we optimized the optimal Dox loading conditions by fixing the DOX concentration (1 mg/mL) and changing the selenium-doped HA weight and by fixing the selenium-doped HA weight (5 mg) and changing the DOX concentration. As can be seen from Figure 4d, when the Dox concentration was fixed at 1 mg/mL, the Dox encapsulation efficiency increased with the increase of the selenium-doped HA weight until its weight reached 5 mg, that is, 0.1Se-n-HA and 0.1Se-m-HA would reach the maximum Dox encapsulation efficiency at this point. From Figure 4e, when the selenium-doped HA mass was 5 mg, the Dox encapsulation efficiency presented a trend of first increasing and then decreasing with the increase of Dox concentration and reached its maximum value when the Dox concentration was 1 mg/mL. These results indicated that the best encapsulation efficiency could be obtained when the Dox concentration was 1 mg/mL and the selenium-doped HA weight was 5 mg. The results also suggested that 0.1Se-n-HA showed a higher encapsulation efficiency (maximum 95%) and

effective drug loading ability compared to 0.1Se-m-HA (maximum 78%) under the same conditions (Figure 4d,e). Based on the above results, we kept the weight of different HA (n-HA, m-HA, 0.1Se-n-HA and 0.1Se-m-HA) at 5 mg and the Dox concentration at 1 mg/mL to explore the effect of selenium doping on the Dox loading capability of different HA. The results in Figure 4f showed that the encapsulation efficiency of Dox in selenium-doped HA was significantly higher than that in selenium-free HA, and 0.1Se-n-HA had a much better Dox loading ability than 0.1Se-m-HA, which was consistent with the previous results.

2.4. Surface Area and Zeta Potential. Specific surface area is always thought of a very important parameter for drug carriers, and the specific surface areas of n-HA, 0.1Se-n-HA, 0.1Se-n-HA-D, m-HA, 0.1Se-m-HA, and 0.1Se-m-HA-D were assessed by Brunauer–Emmett–Teller (BET) and are listed in Table 1. The results in the table show that even with selenium doping and Dox addition, spherical m-HA had a larger BET specific surface area than rod-shaped n-HA. Selenium doping increased the BET value, which further confirmed the view that selenium doping would reduce the HA size and then bring a bigger specific surface area. Dox loading decreased the BET value, which should be related to the Dox loading filling the pores of the samples. Unexpectedly, m-HA possessed a just slightly higher Dox loading efficiency than n-HA but showed a specific surface area more than 3 times than that of n-HA. What is also incredible is that the Dox loading efficiency of 0.1Se-m-HA is just 70% of 0.1Se-n-HA, but its specific surface area is significantly higher than that of 0.1Se-n-HA. These results suggested that the specific surface area of materials should not be the only factor for drug loading; some other parameters of materials may play a more important role.

The nitrogen adsorption and desorption isotherms (Figure 5a–f) show that all the samples had isothermal curves of type 3. The relative pressure of n-HA, 0.1Se-n-HA, and 0.1Se-n-HA-D was 0.5–1, and the relative pressure of m-HA, 0.1Se-m-HA, and 0.1Se-m-HA-D was 0.75–1, which indicated that as shown in schematic diagrams (Figure 5g–j), the reason for the formation of pores in n-HA, 0.1Se-n-HA, and 0.1Se-n-HA-D was particle stacking, while the reason for the formation of pores in m-HA, 0.1Se-m-HA, and 0.1Se-m-HA-D was particle stacking and assembly of HA whiskers. As can be seen from Figure 5a₁–f₁, except for n-HA, the pore diameter of 0.1Se-n-HA, 0.1Se-n-HA-D, m-HA, 0.1Se-m-HA, and 0.1Se-m-HA-D mainly distributed at 10–50 nm, while the pore diameter of n-HA mainly distributed at 130–170 nm. At the same time, it can also be found that doping selenium reduced the pore diameter, and the pore sizes further decreased after loading Dox. The obvious decrease of pore diameter after selenium doping should be attributed to the decrease of HA particle size, which led to a larger specific surface area generating and made agglomeration easier and more compact. The decrease in pore sizes after loading Dox should be attributed to Dox molecules filling these pores. In detail, for 0.1Se-n-HA, the ultrasmall pores (2–6 nm) completely disappeared, and the amounts of pores with different sizes reduced to some extent; even the reduced amount of the pores with a larger diameter (about 150 nm) was more than half, indicating that all the pores with

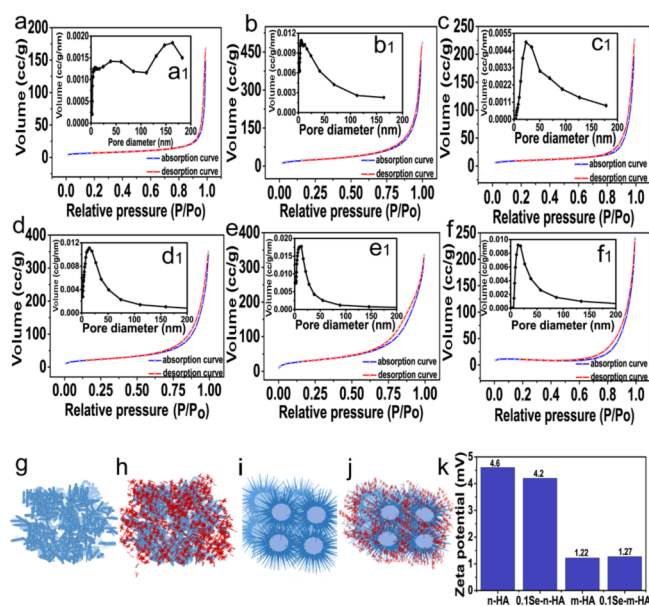


Figure 5. Nitrogen adsorption and desorption isotherms of n-HA (a), 0.1Se-n-HA (b), 0.1Se-n-HA-D (c), m-HA (d), 0.1Se-m-HA (e), and 0.1Se-m-HA-D (f) and their pore size distribution, respectively (a₁–f₁); schematic diagrams of pore distribution in n-HA (g), n-HA-D (h), m-HA (i), and m-HA-D (j); zeta potential of n-HA, 0.1Se-n-HA, m-HA, and 0.1Se-m-HA in water (k).

different sizes in 0.1Se-n-HA contributed to the Dox loading process. However, for 0.1Se-m-HA, although the ultrasmall pores (2–6 nm) also disappeared after Dox loading and the amounts of pores with sizes below 40 nm decreased to a certain extent, the number of pores larger than 40 nm did not decrease significantly, suggesting that only the pores smaller than 40 nm in 0.1Se-m-HA played indeed a role in the Dox loading process. The above difference between 0.1Se-n-HA and 0.1Se-m-HA should also be attributed to the difference in pore structures of them. n-HA and 0.1Se-n-HA will easily aggregate together in the Dox solution, and a number of pores formed by particle stacking are crisscross and suitable for Dox loading. However, for m-HA and 0.1Se-m-HA, they have a sea urchin-like structure formed by self-assembly of whiskers. The pore structure in m-HA and 0.1Se-m-HA should contain two parts; one is the larger spherical space formed in the middle of the microsphere after the whisker self-assembly, and the other is the gap between the whiskers arranged radially. The closer the whisker is to the center of the microsphere, the smaller the gap between whiskers will be, and the smallest gap in m-HA and 0.1Se-m-HA should be smaller than the molecular size of Dox so that Dox cannot be loaded into the middle spherical space of m-HA and 0.1Se-m-HA, that is, the pores in m-HA and 0.1Se-m-HA that really carry Dox should only be the gaps between the whiskers arranged radially. Besides, the size of such gaps gradually increases outward, so when closer to the outside, the Dox loaded is easier to fall off, and only the gaps near the center of the sphere can play a role in drug loading. These should be the reasons why the amounts of pores with a larger size in m-HA and 0.1Se-m-HA do not change significantly and also explained why m-HA possessed a just slightly higher Dox loading efficiency than n-HA but showed a specific surface area more than 3 times that of n-HA and why the Dox loading efficiency of 0.1Se-m-HA is just 70% of

0.1Se-n-HA but its specific surface area is significantly higher than that of 0.1Se-n-HA.

The zeta potential not only affects particles' stability in solution but also plays an important role in drug loading. From Figure 5k, the zeta potentials of n-HA, 0.1Se-n-HA, m-HA, and 0.1Se-m-HA were +4.6, +4.2, +1.22, and +1.27 mV in water, respectively. The results showed that the introduction of selenium did not change the zeta potential of HA significantly, indicating the similar particles' stability of 0.1Se-n-HA and 0.1Se-m-HA with n-HA and m-HA, respectively. The zeta potential absolute value of n-HA and 0.1Se-n-HA was significantly higher than that of m-HA and 0.1Se-m-HA, which implies that n-HA and 0.1Se-n-HA could disperse better driven by mutual repulsion and would have more chance to contact more Dox molecules. In addition, the zeta potential may reflect the state of the HA crystalline surface, which will also affect its adsorption property. The solution of Dox HCl is acidic; when HA is added to the Dox HCl aqueous solution for drug loading, the existing OH⁻ on the HA crystalline surface is easily ionized and then neutralized by H⁺ in the Dox solution, and the ion vacancy of OH⁻ will make the HA crystal to be positively charged and to form an adsorption site for the carboxyl group of Dox.^{48,49} The higher positive value of HA indicates the more OH⁻ vacancy on the HA crystalline surface, which would provide more sites for Dox adsorption. Also, Zhao et al. indicated that the loading of the drug to HA is mainly through the formation of Ca–O bonds between Ca ions on the surface of HA and “O” atoms in the drug molecule,⁵⁰ and the more the ion vacancy of OH⁻, the more the sites of Ca exposure. In the present study, the zeta potentials of the four samples were all positive in weakly acidic deionized water, and the zeta potential absolute value of n-HA and 0.1Se-n-HA was significantly higher than that of m-HA and 0.1Se-m-HA, suggesting more OH⁻ vacancy on the crystalline surface of n-HA and 0.1Se-n-HA. These results suggested that the formation of more Dox adsorption sites may be one of reasons why 0.1Se-n-HA showed a high Dox load capacity with a low specific surface area.

Therefore, the materials with larger specific surface areas do not always imply that a higher drug loading capacity and the drug loading ability of materials should be codetermined by the material specific surface area, pore structure, and other parameters (e.g., charge properties and functional groups on the material surface).

2.5. Release of Selenium and Dox. A controllable drug release is a primary requirement for a drug delivery system. Here, in order to simulate the weakly acidic environment of the tumor and the acid environment of the lysosome, we explored the release behavior of selenium and Dox in PBS with pH values of 5 and 6.8, and the results are shown in Figure 6. It can be found from Figure 6a–d that the release behavior of Dox from two morphological HA (n-HA-D and m-HA-D) presented a similar trend, which experienced relatively rapid release in the first 12 h and showed a slow release behavior in the later period. It can also be found that the pH value of the PBS solution affects the Dox release remarkably; the lower the pH value of PBS, the faster the release of Dox. The release amounts of Dox were about 40 μg from n-HA-D and 60 μg from m-HA-D in the first hour in the PBS solution of pH = 5, while the release amounts of Dox were about 25 μg from n-HA-D and 40 μg from m-HA-D in the PBS solution of pH = 6.8 within the first hour. Interestingly, the accumulative release amount of Dox from m-HA-D was always slightly higher than

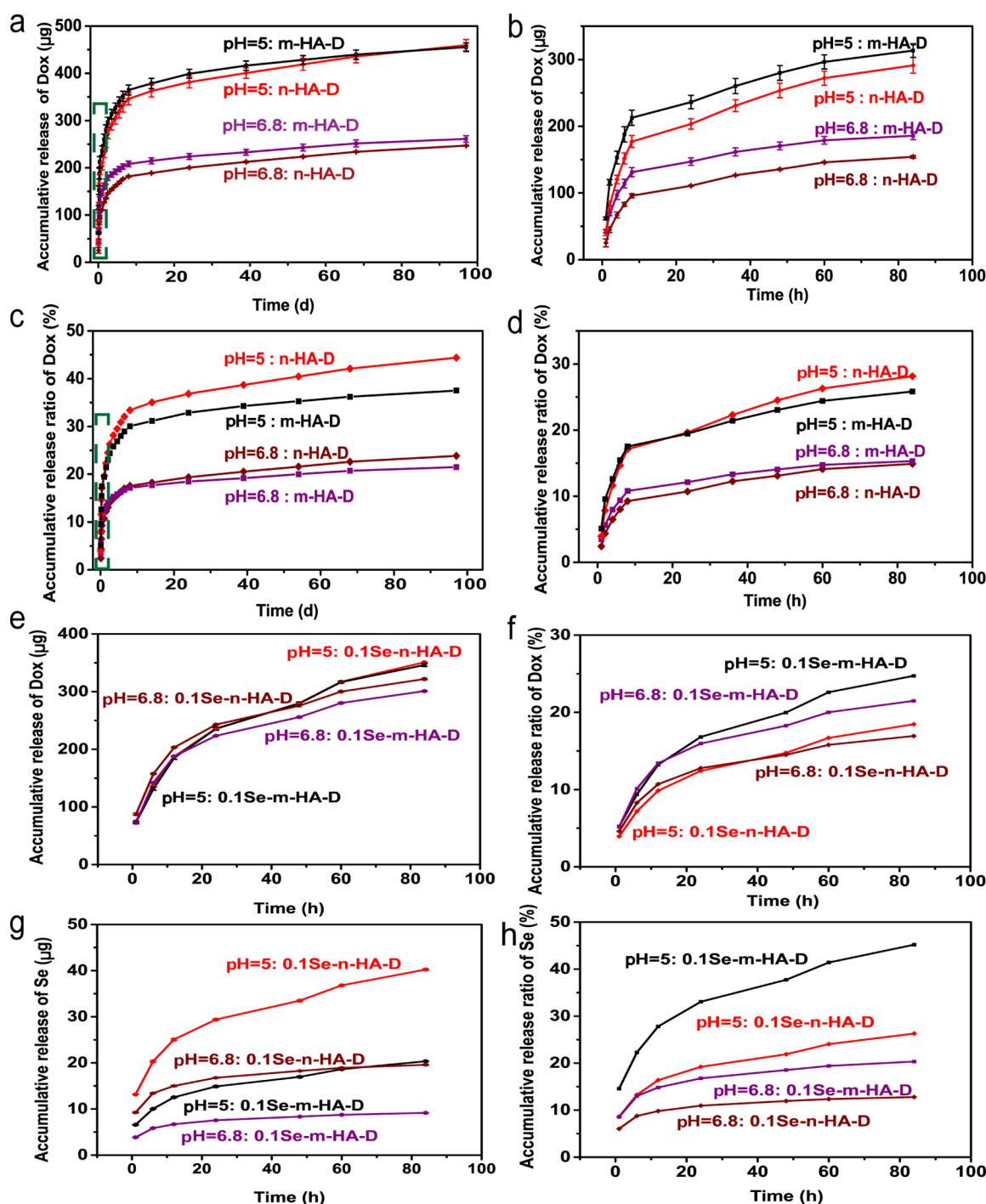


Figure 6. Dox accumulative release amount (a) and Dox accumulative release ratio (c) of n-HA-D and m-HA-D in PBS with a pH of 5 or 6.8; Dox release in the first 84 h in (a,c) were magnified in (b,d), respectively; Dox accumulative release amount (e), Dox accumulative release ratio (f), selenium release amount (g), and selenium release ratio (h) of 0.1Se-n-HA-D and 0.1Se-m-HA-D in PBS with a pH of 5 or 6.8.

that from n-HA-D in all 97 days of drug release time. Notably, after 64 days of release, the m-HA-D group showed a relatively flat platform phase, while the n-HA-D group showed a continuous release profile. After 97 days, the accumulative Dox release ratios of n-HA-D and m-HA-D were about 45% and 35% in PBS with pH = 5 and were about 23% and 21% in PBS with pH = 6.8, respectively (Figure 6c). Although, the accumulative release ratio of Dox from n-HA-D was slightly higher than that from m-HA-D on the whole, the former was

slightly lower than the latter before 24 h release in PBS with pH = 5 and before 84 h release in PBS with pH = 6.8.

The Dox release behaviors in selenium-doped HA-D (0.1Se-n-HA-D and 0.1Se-m-HA-D) and non-selenium-doped HA-D (n-HA-D and m-HA-D) were compared to explore whether the selenium doping would affect the release of Dox. Figure 6e,f shows that there was no significant difference of Dox releasing amount between 0.1Se-n-HA-D and 0.1Se-m-HA-D (about 350 μg in PBS with pH = 5 and 300 μg in PBS with pH = 6.8) after 84 h release; however, these Dox releasing

amounts were higher than those of n-HA-D and m-HA-D in the same release period. The Dox releasing ratio of 0.1Se-m-HA-D (about 25% in PBS with pH = 5 and 20% in PBS with pH = 6.8) was higher than the Dox releasing ratio of 0.1Se-n-HA-D (about 17% in PBS with pH = 5 and 15% in PBS with pH = 6.8), and the reason may be attributed to the fact that 0.1Se-m-HA-D had more bigger pores, which is conducive to Dox releasing. These results indicated that the Dox releasing amount from 0.1Se-n-HA-D and 0.1Se-m-HA-D was higher than Dox from n-HA-D and m-HA-D. The Dox releasing ratio of m-HA-D in PBS of pH = 5 or pH = 6.8 was almost the same with 0.1Se-m-HA-D correspondingly, and the Dox releasing ratio of 0.1Se-n-HA-D was lower than that of n-HA-D, m-HA-D, and 0.1Se-m-HA-D in PBS of pH = 5, which exhibited a better Dox-controlled release behavior of 0.1Se-n-HA-D.

There was a worry that excessive Dox remaining in the body for a long time would cause a damage to normal tissues. Previous research reported that Dox concentrations maintained at 400–1000 ng/mL around the implanting site and 100–400 ng/mL in the blood can satisfy tissue recovery after 12 weeks and inhibit osteosarcoma recurrence within 1 to 12 months.⁵¹ In addition, some studies illustrated that the concentration of Dox at 1–5 $\mu\text{g}/\text{mL}$ can inhibit and kill osteosarcoma cells.^{52,53} In the current study, the Dox concentration released from 5 mg of HA in 4 mL of PBS could averagely reach 1 $\mu\text{g}/\text{mL}$ per day in the first 54 days and then maintain at about 100 ng per day, which suggested that n-HA-D, m-HA-D, 0.1Se-n-HA-D, and 0.1Se-m-HA-D had potential to inhibit osteosarcoma safely and efficiently.

The release behavior of selenium (Figure 6g,h) showed that the Se release amount of 0.1Se-n-HA-D (about 40 μg in PBS with pH = 5 and 20 μg in PBS with pH = 6.8) was higher than that of 0.1Se-m-HA-D (about 20 μg in PBS with pH = 5 and 10 μg in PBS with pH = 6.8), but the Se release ratio of 0.1Se-m-HA-D (about 45% in PBS with pH = 5 and 20% in PBS with pH = 6.8) was higher than that of 0.1Se-n-HA-D (about 25% in PBS with pH = 5 and 10% in PBS with pH = 6.8). These results indicated that the release behavior of Se from 0.1Se-n-HA-D and 0.1Se-m-HA-D may be responsive to pH, which showed a probably trend that the lower the pH of the PBS solution, the faster the speed and the greater the quantities of Se released. Although the Se release behaviors were similar in 0.1Se-n-HA-D and 0.1Se-m-HA-D, the release amount of Se from 0.1Se-n-HA-D was twice as much as that from 0.1Se-m-HA-D, which was attributed to the higher selenium doping content in 0.1Se-n-HA-D than in 0.1Se-m-HA-D. The release amounts of Se ranged at 0–40 μg , suggesting that the selenium release amount was lower than the toxic dose for humans (no more than 90 $\mu\text{g}/\text{d}$ per person).⁵⁴ In addition, articles have reported that the IC_{50} dose of Se inhibiting tumor cells was around 15 $\mu\text{g}/\text{mL}$ from selenium-doped calcium phosphate⁵⁵ and 2.56 $\mu\text{g}/\text{mL}$ from sodium selenite solution,⁵⁶ and these results indicated that the selenium-doped HA (0.1Se-n-HA, 0.1Se-m-HA, 0.1Se-n-HA-D, and 0.1Se-m-HA-D) has anti-tumor potential.

Selenium is an essential trace element in the human body, and studies have shown that a certain concentration of selenium is beneficial for the proliferation of BMSCs and is unfavorable for the proliferation of MG63, one of the human osteosarcoma cells.¹² Another study reported that sodium selenite (Na_2SeO_3) with 10–40 $\mu\text{mol}/\text{L}$ could inhibit the proliferation and improve apoptosis of human osteosarcoma U-2OS cells.⁵⁷ Studies also presented the potential of selenium

in anti-osteosarcoma, where the mechanism of selenium against osteosarcoma is its capacity of prompting oxidative damage of DNA and mitochondria, leading to mitochondrial dysfunctions.⁵⁸ According to the previous literature, 0.1Se-n-HA-D and 0.1Se-m-HA-D fabricated in the current study may have potential in anti-osteosarcoma applications.

3. CONCLUSIONS

In this study, selenium-doped rod-shaped n-HA and spherical mesoporous m-HA were successfully prepared. The doping efficiency of selenium, the Dox loading, and release behaviors of selenium-doped HA with different morphologies were systematically studied. The results showed that the rod-like n-HA had higher Se doping efficiency, higher Dox loading capacity, and more ideal Se and Dox-sustained release behavior. Therefore, the sustained release system of Se-doped n-HA loaded with Dox has great potential in the field of bone regeneration and prevention of recurrence of osteosarcoma.

4. MATERIALS AND METHODS

4.1. Materials. Sodium creatine phosphate tetrahydrate ($\text{C}_4\text{H}_8\text{Na}_2\text{O}_3\text{P}\cdot 4\text{H}_2\text{O}$) and Dox HCl ($\text{C}_{27}\text{H}_{29}\text{NO}_{11}\cdot\text{HCl}$) were obtained from Meilun Biotechnology Co., Ltd. (Dalian, China). Sodium hydroxide (NaOH), disodium hydrogen phosphate dodecahydrate ($\text{Na}_2\text{HPO}_4\cdot 12\text{H}_2\text{O}$), and calcium nitrate tetrahydrate [$\text{Ca}(\text{NO}_3)_2\cdot 4\text{H}_2\text{O}$] were purchased from Chengdu Kelong Chemical Reagent Factory (Chengdu, China). Calcium chloride dihydrate ($\text{CaCl}_2\cdot 2\text{H}_2\text{O}$) was bought from Shanghai Weiting Biotechnology Co., Ltd. (Shanghai, China). Sodium selenite (Na_2SeO_3) was purchased from Sinopharm Group Chemical Reagent Co., Ltd. (Shanghai, China).

4.2. HA and Selenium-Doped HA Preparation. Nano-HA was synthesized by a wet chemical method. Briefly, 0.5 mol L^{-1} aqueous solution of $\text{Ca}(\text{NO}_3)_2\cdot 4\text{H}_2\text{O}$ was dropped into an equal volume of 0.3 mol L^{-1} ($\text{Na}_2\text{HPO}_4\cdot 12\text{H}_2\text{O}$) solution with continuous stirring at 70–80 $^\circ\text{C}$, and the pH value was controlled at about 10 with sodium hydroxide. After the solution was dripped, the reaction system was stirred continuously for another 2 h. Subsequently, after freeze-drying for 48 h, the obtained precipitate was ground and sieved via a 400 mesh sieve. For preparation of selenium-substituted n-HA (0.1Se-n-HA), Na_2SeO_3 together with $\text{Na}_2\text{HPO}_4\cdot 12\text{H}_2\text{O}$ was used in the preparation process. The total molarity of P and Se was controlled to be consistent with the molarity of the P element in the preparation of n-HA, in which the molar ratio of Se to P was controlled at 0.1, and other conditions were kept consistent with the n-HA preparation.

m-HA was synthesized by a microwave hydrothermal method. Briefly, 100 mL of an aqueous solution of 0.06 mol L^{-1} phosphocreatine ($\text{C}_4\text{H}_8\text{Na}_2\text{O}_3\text{P}\cdot 4\text{H}_2\text{O}$) was dropped into 300 mL of 0.0333 mol L^{-1} $\text{CaCl}_2\cdot 2\text{H}_2\text{O}$ aqueous solution with continuous stirring, and the pH was adjusted to around 10 by using sodium hydroxide. After the solution finished dripping, the mixture needed stirring for another hour. Subsequently, the mixture was then transferred to a microwave reactor, and microwave-assisted hydrothermal synthesis was performed for 30 min at 120 $^\circ\text{C}$ and 5 W. Then, the obtained precipitate was washed with deionized water, and the m-HA powder was obtained after freeze-drying for 48 h; then grinding and sieving via a 400 mesh sieve. To prepare selenium-substituted m-HA

(0.1Se-m-HA), Na_2SeO_3 and other reactants were added in the mixture together. The total molarity of P and Se was controlled to be consistent with the molarity of the P element in the preparation process of m-HA; the molar ratio of Se to P was also controlled at 0.1, and other conditions were kept consistent with the m-HA preparation.

4.3. Physicochemical Characterization. The morphology of synthesized HA particle was observed by SEM (JSM-7500F, Japan) and TEM (Tecnai G2 F20 S-TWIN, US). The particle size (100 particles were randomly picked) was calculated from the TEM images by Image Pro software. The phase identification and components of resultant products were characterized by XRD (EMPYREAN, The Netherlands) and FTIR spectroscopy (Nicolet 6700, USA).

The presence of selenium in the particles was examined by EDS (X-MaxN 20, Oxford, UK) and XPS (AXIS Supra, Kratos, British). The amount of selenium doped in 0.1Se-n-HA or 0.1Se-m-HA was measured by ICP-MS (VG PQExCell, USA). In detail, 0.1Se-n-HA or 0.1Se-m-HA particles were dissolved in 0.1 mol L^{-1} nitric acid solution to obtain 0.001 mg/mL 0.1Se-n-HA solution or 0.1Se-m-HA solution; then, the selenium concentration of the prepared solution was determined by ICP-MS. The selenium content in 0.1Se-n-HA and 0.1Se-m-HA particles was further measured using an XRF spectrometer (XRF-1800, Japan) to verify the results of ICP-MS.

The specific surface area and pore diameter of different HA were measured using a BET instrument (Kubo-X1000, Beijing). The surface charge of HA in aqueous solution was characterized using a Malvern Zetasizer nano instrument (Zen 3600, UK).

4.4. Dox Loading. Dox was loaded onto n-HA, m-HA, 0.1Se-n-HA, or 0.1Se-m-HA by a solution impregnation oscillation method. Briefly, 5 mg of n-HA, m-HA, 0.1Se-n-HA, and 0.1Se-m-HA were added to a brown glass bottle containing 2 mL of 1 mg/mL Dox solution, oscillated at 5 Hz for 72 h under dark conditions ($n = 6$), and centrifuged at 10,000 rpm for 20 min, and the resulting precipitations were denoted as n-HA-D, m-HA-D, 0.1Se-n-HA-D, and 0.1Se-m-HA-D. The maximum absorption wavelength of Dox was 481 nm in water and 482 nm in the PBS buffer (pH = 5 and pH = 6.8), measured using a UV-vis-near-infrared spectrophotometer (UV, UV-3600, Japan). The standard curves of Dox absorbance-concentration in water and PBS were plotted by configuring Dox solutions with a concentration gradient ($n = 6$). The Dox concentration in the supernatant was obtained through the measurement of its absorbance at 481 nm and denoted as C_t . The drug encapsulation rate were calculated by the following formula

$$\text{drug encapsulation rate (\%)} = \frac{C_0 - C_t}{C_0} \cdot 100\%$$

where C_0 is the initial concentration of Dox and C_t is the Dox concentration in the supernatant.

4.5. Release of Selenium and Dox in PBS. The release behavior of selenium and Dox in the PBS buffer at pH = 6.8 or pH = 5 was investigated to simulate the tumor slight acidic environment and the lysosomal environment. In detail, 5 mg of n-HA-D, 5 mg of m-HA-D, 5 mg of 0.1Se-n-HA-D, and 5 mg of 0.1Se-m-HA-D were added into 4 mL of the PBS buffer at pH = 6.8 or 5 ($n = 4$) and oscillated continuously at 2 Hz until the predetermined time point was reached. Then, the samples

were centrifuged at 4000 rpm for 20 min, all supernatant was taken out for the measurement, and another 4 mL of fresh PBS was added into each sample for the next drug release. Finally, the accumulative release amount of Dox at each predetermined time point was determined according the absorbance of the supernatant at 482 nm via a UV spectrophotometer, and the accumulative release ratio of Dox was further calculated through dividing the accumulative release amount of Dox by the initial Dox amount in 5 mg of n-HA-D, 5 mg of m-HA-D, 5 mg of 0.1Se-n-HA-D, and 5 mg of 0.1Se-m-HA-D. The accumulative release amount of the selenium element was determined by ICP-MS, and the accumulative release ratio of the selenium element was further calculated through dividing the accumulative release amount of selenium by the initial selenium amount in 10 mg of 0.1Se-n-HA or 10 mg of 0.1Se-m-HA.

4.6. Statistical Analysis. Statistical analysis was performed using Origin 9.1 software, and quantitative data were expressed as the mean \pm standard deviation.

AUTHOR INFORMATION

Corresponding Authors

Yi Zuo – Research Center for Nano Biomaterials, Analytical & Testing Center, Sichuan University, Chengdu 610064, P. R. China; orcid.org/0000-0003-2301-9786; Phone: +86 28 85418178; Email: zoe@vip.sina.com, zoe@scu.edu.cn; Fax: +86 28 85418178

Jidong Li – Research Center for Nano Biomaterials, Analytical & Testing Center, Sichuan University, Chengdu 610064, P. R. China; Email: nic1979@scu.edu.cn

Authors

Jing Gao – Research Center for Nano Biomaterials, Analytical & Testing Center, Sichuan University, Chengdu 610064, P. R. China; orcid.org/0000-0002-3382-1222

Jinhui Huang – Research Center for Nano Biomaterials, Analytical & Testing Center, Sichuan University, Chengdu 610064, P. R. China

Rui Shi – Department of Orthopaedics, West China Hospital, Sichuan University, Chengdu 610041, PR China

Jiawei Wei – Research Center for Nano Biomaterials, Analytical & Testing Center, Sichuan University, Chengdu 610064, P. R. China

Xiaoyu Lei – Research Center for Nano Biomaterials, Analytical & Testing Center, Sichuan University, Chengdu 610064, P. R. China

Yichen Dou – Research Center for Nano Biomaterials, Analytical & Testing Center, Sichuan University, Chengdu 610064, P. R. China

Yubao Li – Research Center for Nano Biomaterials, Analytical & Testing Center, Sichuan University, Chengdu 610064, P. R. China

Complete contact information is available at:

<https://pubs.acs.org/10.1021/acsomega.1c00092>

Notes

The authors declare no competing financial interest.

ACKNOWLEDGMENTS

This research was financially supported by the National Key Research and Development Program of China (2017YFC1104303) and the Key Applied Basic Research Program of Sichuan Province, China (2018JY0031). We

gratefully acknowledge Jiqui Wen (Analytical and Testing Center of Sichuan University) for the help of the XRD measurement and Xi Wu (Analytical and Testing Center of Sichuan University) for the help of the ICP–MS test.

REFERENCES

- (1) Zhang, C.; Morimoto, L. M.; de Smith, A. J.; Hansen, H. M.; Gonzalez-Maya, J.; Endicott, A. A.; Smirnov, I. V.; Metayer, C.; Wei, Q.; Eward, W. C.; Wiemels, J. L.; Walsh, K. M. Genetic determinants of childhood and adult height associated with osteosarcoma risk. *Cancer* **2018**, *124*, 3742–3752.
- (2) Mirabello, L.; Pfeiffer, R.; Murphy, G.; Daw, N. C.; Patiño-García, A.; Troisi, R. J.; Hoover, R. N.; Douglass, C.; Schüz, J.; Craft, A. W.; Savage, S. A. Height at diagnosis and birth-weight as risk factors for osteosarcoma. *Cancer Causes Control* **2011**, *22*, 899–908.
- (3) Júnior, R. Z. B.; Camargo, O. P. Prognostic factors in the survival of patients diagnosed with primary non-metastatic osteosarcoma with a poor response to neoadjuvant chemotherapy. *Clinics* **2009**, *64*, 1177–1186.
- (4) Liang, L.; Zhang, T.; You, Y.; He, Q.; Fan, Y.; Liao, G. An individual patient data meta-analysis on the effect of chemotherapy on survival in patients with craniofacial osteosarcoma. *Head Neck J. Sci. Spec.* **2019**, *41*, 2016–2023.
- (5) Botter, S. M.; Neri, D.; Fuchs, B. Recent advances in osteosarcoma. *Curr. Opin. Pharmacol.* **2014**, *16*, 15–23.
- (6) Chen, C.; Lu, L.; Yan, S.; Yi, H.; Yao, H.; Wu, D.; He, G.; Tao, X.; Deng, X. Autophagy and doxorubicin resistance in cancer. *Anti-Cancer Drugs* **2018**, *29*, 1–9.
- (7) Zhu, K.-P.; Zhang, C.-L.; Ma, X.-L.; Hu, J.-P.; Cai, T.; Zhang, L. Analyzing the Interactions of mRNAs and ncRNAs to Predict Competing Endogenous RNA Networks in Osteosarcoma Chemo-Resistance. *Mol. Ther.* **2019**, *27*, 518–530.
- (8) Zhang, C.-L.; Zhu, K.-P.; Ma, X.-L. Antisense lncRNA FOXC2-AS1 promotes doxorubicin resistance in osteosarcoma by increasing the expression of FOXC2. *Canc. Lett.* **2017**, *396*, 66–75.
- (9) Schroeder, C. P.; Goeldner, E. M.; Schulze-Forster, K.; Eickhoff, C. A.; Holtermann, P.; Heidecke, H. Effect of selenite combined with chemotherapeutic agents on the proliferation of human carcinoma cell lines. *Biol. Trace Elem. Res.* **2004**, *99*, 017–026.
- (10) Wang, Y.; Wang, J.; Hao, H.; Cai, M.; Wang, S.; Ma, J.; Li, Y.; Mao, C.; Zhang, S. In Vitro and in Vivo Mechanism of Bone Tumor Inhibition by Selenium-Doped Bone Mineral Nanoparticles. *ACS Nano* **2016**, *10*, 9927–9937.
- (11) Wang, Y.; Hao, H.; Liu, H.; Wang, Y.; Li, Y.; Yang, G.; Ma, J.; Mao, C.; Zhang, S. Selenium-Releasing Bone Mineral Nanoparticles Retard Bone Tumor Growth and Improve Healthy Tissue Functions In Vivo. *Adv. Healthcare Mater.* **2015**, *4*, 1813–1818.
- (12) Wang, Y.; Ma, J.; Zhou, L.; Chen, J.; Liu, Y.; Qiu, Z.; Zhang, S. Dual functional selenium-substituted hydroxyapatite. *Interface Focus* **2012**, *2*, 378–386.
- (13) Wang, Y.; Liu, X.; Deng, G.; Sun, J.; Yuan, H.; Li, Q.; Wang, Q.; Lu, J. Se@SiO₂-FA-CuS nanocomposites for targeted delivery of DOX and nano selenium in synergistic combination of chemotherapeutic therapy. *Nanoscale* **2018**, *10*, 2866–2875.
- (14) Caffrey, P. B.; Frenkel, G. D. Sensitivity of melphalan-resistant tumors to selenite in vivo. *Canc. Lett.* **1997**, *121*, 177–180.
- (15) Bacci, G.; Longhi, A.; Bertoni, F.; Bacchini, P.; Ruggeri, P.; Versari, M.; Picci, P. Primary High-Grade Osteosarcoma. *J. Pediatr. Hematol./Oncol.* **2005**, *27*, 129–134.
- (16) Zheng, P.; Liu, Y.; Chen, J.; Xu, W.; Li, G.; Ding, J. Targeted pH-responsive polyion complex micelle for controlled intracellular drug delivery. *Chin. Chem. Lett.* **2020**, *31*, 1178–1182.
- (17) Zhang, Y.; Cai, L.; Li, D.; Lao, Y.-H.; Liu, D.; Li, M.; Ding, J.; Chen, X. Tumor microenvironment-responsive hyaluronate-calcium carbonate hybrid nanoparticle enables effective chemotherapy for primary and advanced osteosarcomas. *Nano Res.* **2018**, *11*, 4806–4822.
- (18) Jayaraman, P.; Gandhimathi, C.; Venugopal, J. R.; Becker, D. L.; Ramakrishna, S.; Srinivasan, D. K. Controlled release of drugs in electrospayed nanoparticles for bone tissue engineering. *Adv. Drug Deliv. Rev.* **2015**, *94*, 77–95.
- (19) Huang, H.; Du, M.; Chen, J.; Zhong, S.; Wang, J. Preparation and characterization of abalone shells derived biological mesoporous hydroxyapatite microspheres for drug delivery. *Mater. Sci. Eng. C* **2020**, *113*, 110969.
- (20) Wang, Y.-H.; Hao, H.; Wu, J. X.; Yao, Y.; Qin, N.; He, W. C. Enhanced Antitumor Effect and Drug Delivery from Se Doped Hydroxyapatite Microspheres. *Chin. J. Inorg. Chem.* **2018**, *34*, 1517–1530.
- (21) Zhang, H.; Dong, S.; Li, Z.; Feng, X.; Xu, W.; Tuliniao, C. M. S.; Jiang, Y.; Ding, J. Biointerface engineering nanoplatforams for cancer-targeted drug delivery. *Asian J. Pharm. Sci.* **2020**, *15*, 397–415.
- (22) Ding, J.; Chen, J.; Gao, L.; Jiang, Z.; Zhang, Y.; Li, M.; Xiao, Q.; Lee, S. S.; Chen, X. Engineered nanomedicines with enhanced tumor penetration. *Nano Today* **2019**, *29*, 100800.
- (23) Zhao, D.; Zhu, T.; Li, J.; Cui, L.; Zhang, Z.; Zhuang, X.; Ding, J. Poly (lactic-co-glycolic acid)-based composite bone-substitute materials. *Bioact. Mater.* **2021**, *6*, 346–360.
- (24) Winkler, T.; Sass, F. A.; Duda, G. N.; Schmidt-Bleek, K. A review of biomaterials in bone defect healing, remaining shortcomings and future opportunities for bone tissue engineering THE UNSOLVED CHALLENGE. *Bone Joint Res.* **2018**, *7*, 232–243.
- (25) Souza, E. Q. M.; Costa Klaus, A. E.; Espósito Santos, B. F.; Carvalho da Costa, M.; Ervolino, E.; Coelho de Lima, D.; Fernandes, L. A. Evaluations of hydroxyapatite and bioactive glass in the repair of critical size bone defects in rat calvaria. *J. Oral Biol. Craniofac. Res.* **2020**, *10*, 422–429.
- (26) Fernandes, M. H.; Alves, M. M.; Cebotarencu, M.; Ribeiro, I. A. C.; Grenho, L.; Gomes, P. S.; Carmezim, M. J.; Santos, C. F. Citrate zinc hydroxyapatite nanorods with enhanced cytocompatibility and osteogenesis for bone regeneration. *Mater. Sci. Eng. C* **2020**, *115*, 111147.
- (27) Zhang, K.; Zhou, Y.; Xiao, C.; Zhao, W.; Wu, H.; Tang, J.; Li, Z.; Yu, S.; Li, X.; Min, L.; Yu, Z.; Wang, G.; Wang, L.; Zhang, K.; Yang, X.; Zhu, X.; Tu, C.; Zhang, X. Application of hydroxyapatite nanoparticles in tumor-associated bone segmental defect. *Sci. Adv.* **2019**, *5*, No. eaax6946.
- (28) Wang, Y.-H.; Hao, H.; Wu, J.; Yao, Y.; Qin, N.; He, W. Enhanced Antitumor Effect and Drug Delivery from Se Doped Hydroxyapatite Microspheres. *Chin. J. Inorg. Chem.* **2018**, *34*, 1517–1530.
- (29) Shi, Z.; Xia, D.; Zeng, G.; Li, X.; Wang, S.; Xu, H. Preparation of nano-hydroxyapatite and evaluation on drug loading properties for doxorubicin. *J. China Pharm. Univ.* **2017**, *34*, 1–6, DOI: DOI: 10.14066/j.cnki.cn21-1349/r.2017.01.00
- (30) Xiao, W.-q.; Zhang, J.; Li, K.; Zou, X.; Cai, Y.; Li, B.; Liu, X.; Xiaoling, L. Litchi-like supermagnetic hydroxyapatite microspheres with hierarchically mesoporous microspheres. *J. Inorg. Mater.* **2019**, *39*, 925–932.
- (31) Li, X.; Wang, Y.; Chen, Y.; Zhou, P.; Wei, K.; Wang, H.; Wang, J.; Fang, H.; Zhang, S. Hierarchically constructed selenium-doped bone-mimetic nanoparticles promote ROS-mediated autophagy and apoptosis for bone tumor inhibition. *Biomaterials* **2020**, *257*, 120253.
- (32) Barbanente, A.; Nadar, R. A.; Esposito, L. D.; Palazzo, B.; Iafisco, M.; van den Beucken, J. J. J. P.; Leeuwenburgh, S. C. G.; Margiotta, N. Platinum-loaded, selenium-doped hydroxyapatite nanoparticles selectively reduce proliferation of prostate and breast cancer cells co-cultured in the presence of stem cells. *J. Mater. Chem. B* **2020**, *8*, 2792–2804.
- (33) Wang, Y.; He, W.; Hao, H.; Wu, J.; Qin, N. Eggshell derived Se-doped HA nanorods for enhanced antitumor effect and curcumin delivery. *J. Sol-Gel Sci. Technol.* **2018**, *87*, 600–607.
- (34) Oledzka, E.; Sobczak, M.; Kolmas, J.; Nalecz-Jawecki, G. Selenium-Substituted Hydroxyapatite/Biodegradable Polymer/Pamidronate Combined Scaffold for the Therapy of Bone Tumour. *Int. J. Mol. Sci.* **2015**, *16*, 22205–22222.

- (35) Zhang, Y.; Wang, F.; Li, M.; Yu, Z.; Qi, R.; Ding, J.; Zhang, Z.; Chen, X. Self-Stabilized Hyaluronate Nanogel for Intracellular Codelivery of Doxorubicin and Cisplatin to Osteosarcoma. *Adv. Sci.* **2018**, *5*, 1700821.
- (36) Kolmas, J.; Pajor, K.; Pajchel, L.; Przekora, A.; Ginalska, G.; Oledzka, E.; Sobczak, M. Fabrication and physicochemical characterization of porous composite microgranules with selenium oxyanions and risedronate sodium for potential applications in bone tumors. *Int. J. Nanomed.* **2017**, *12*, 5633–5642.
- (37) Pajor, K.; Pajchel, L.; Kolodziejska, B.; Kolmas, J. Selenium-Doped Hydroxyapatite Nanocrystals—Synthesis, Physicochemical Properties and Biological Significance. *Crystals* **2018**, *8*, 188.
- (38) Alif, M. F.; Aprillia, W.; Arief, S. A hydrothermal synthesis of natural hydroxyapatite obtained from *Corbicula molitkiana* freshwater clams shell biowaste. *Mater. Lett.* **2018**, *230*, 40–43.
- (39) Ghosh, S.; Ghosh, S.; Jana, S. K.; Pramanik, N. Biomedical Application of Doxorubicin Coated Hydroxyapatite-Poly(lactide-co-glycolide) Nanocomposite for Controlling Osteosarcoma Therapeutics. *J. Nanosci. Nanotechnol.* **2020**, *20*, 3994–4004.
- (40) Sun, J.; Zheng, X.; Li, H.; Fan, D.; Song, Z.; Ma, H.; Hua, X.; Hui, J. Monodisperse selenium-substituted hydroxyapatite: Controllable synthesis and biocompatibility. *Mater. Sci. Eng. C* **2017**, *73*, 596–602.
- (41) Mo, Y.; Vincent, T.; Faur, C.; Guibal, E. Se (VI) sorption from aqueous solution using alginate/polyethylenimine membranes: Sorption performance and mechanism. *Int. J. Biol. Macromol.* **2020**, *147*, 832–843.
- (42) Baek, K.; Ciblak, A.; Mao, X.; Kim, E.-J.; Alshwabkeh, A. Iron anode mediated transformation of selenate in sand columns. *Water Res.* **2013**, *47*, 6538–6545.
- (43) Hortin, J. M.; Anderson, A. J.; Britt, D. W.; Jacobson, A. R.; McLean, J. E. Copper oxide nanoparticle dissolution at alkaline pH is controlled by dissolved organic matter: influence of soil-derived organic matter, wheat, bacteria, and nanoparticle coating. *Environ. Sci. Nano* **2020**, *7*, 2618–2631.
- (44) Liang, J.; Ding, Z.; Qin, H.; Li, J.; Wang, W.; Luo, D.; Geng, R.; Li, P.; Fan, Q. Ultra-fast enrichment and reduction of As (V)/Se (VI) on three dimensional graphene oxide sheets-oxidized carbon nanotubes hydrogels. *Environ. Pollut.* **2019**, *251*, 945–951.
- (45) Geng, R.; Wang, W.; Din, Z.; Luo, D.; He, B.; Zhang, W.; Liang, J.; Li, P.; Fan, Q. Exploring sorption behaviors of Se (IV) and Se (VI) on Beishan granite: Batch, ATR-FTIR, and XPS investigations. *J. Mol. Liq.* **2020**, *309*, 113029.
- (46) Zhang, L.; Li, S.; Li, H.; Pei, L. Bioactive surface modification of carbon/carbon composites with multilayer SiC-SiC nanowire-Si doped hydroxyapatite coating. *J. Alloys Compd.* **2018**, *740*, 109–117.
- (47) Chen, F.; Zhu, Y.-J.; Zhao, X.-Y.; Lu, B.-Q.; Wu, J. Solvothermal synthesis of oriented hydroxyapatite nanorod/nanosheet arrays using creatine phosphate as phosphorus source. *CrystEngComm* **2013**, *15*, 4527–4531.
- (48) Qinyu, C.; Rongrong, Z.; Rui, Z.; Chuan, T.; Xiaoyu, S.; Shilong, W. Preparation and Characterization of Nano-hydroxyapatite as Carrier of Two Drugs. *Fudan Univ. J.* **2009**, *48*, 386–390.
- (49) Deng, C.; Weng, J.; Zhou, S. B.; Lu, X.; Wang, J. X.; Feng, B.; Qu, S. X.; Li, X. H. Review of Surface Adsorption Property of Hydroxyapatite. *Mater. Rev.* **2007**, *21*, 84–87.
- (50) Zhao, Q.; Zhang, D.; Sun, R.; Shang, S.; Wang, H.; Yang, Y.; Wang, L.; Liu, X.; Sun, T.; Chen, K. Adsorption behavior of drugs on hydroxyapatite with different morphologies: A combined experimental and molecular dynamics simulation study. *Ceram. Int.* **2019**, *45*, 19522–19527.
- (51) Wang, Y.; Sun, L.; Mei, Z.; Zhang, F.; He, M.; Fletcher, C.; Wang, F.; Yang, J.; Bi, D.; Jiang, Y.; Liu, P. 3D printed biodegradable implants as an individualized drug delivery system for local chemotherapy of osteosarcoma. *Mater. Des.* **2020**, *186*, 108336.
- (52) Wei, H.; Chen, J.; Wang, S.; Fu, F.; Zhu, X.; Wu, C.; Liu, Z.; Zhong, G.; Lin, J. A Nanodrug Consisting of Doxorubicin And Exosome Derived From Mesenchymal Stem Cells For Osteosarcoma Treatment In Vitro. *Int. J. Nanomed.* **2019**, *14*, 8603–8610.
- (53) Gurunathan, S.; Jeyaraj, M.; Kang, M.-H.; Kim, J.-H. Tangeretin-Assisted Platinum Nanoparticles Enhance the Apoptotic Properties of Doxorubicin: Combination Therapy for Osteosarcoma Treatment. *Nanomaterials* **2019**, *9*, DOI: DOI: 10.3390/nano9081089
- (54) Al-Othman, A. M.; Al-Othman, Z. A.; El-Desoky, G. E.; Aboul-Soud, M. A. M.; Habila, M. A.; Giesy, J. P. Daily intake of selenium and concentrations in blood of residents of Riyadh City, Saudi Arabia. *Environ. Geochem. Health* **2012**, *34*, 417–431.
- (55) Hu, J.; Jiang, Y.; Tan, S.; Zhu, K.; Cai, T.; Zhan, T.; He, S.; Chen, F.; Zhang, C. Selenium-doped calcium phosphate biomineral reverses multidrug resistance to enhance bone tumor chemotherapy. *Nanomedicine* **2021**, *32*, 102322.
- (56) Qin, Y.; Xu, H.; Xu, J.; Gu, M.; Wei, Y. Cytotoxicity in Human Colon Adenocarcinoma Caco-2 Cell Induced by Selenite and Selenomethionine. *Xiandai Shipin Keji* **2021**, *37*, 1–6.
- (57) Chen, X.-j.; Duan, F.-d.; Zhang, H.-h.; Xiong, Y.; Wang, J. Sodium selenite-induced apoptosis mediated by ROS attack in human osteosarcoma U2OS cells. *Biol. Trace Elem. Res.* **2012**, *145*, 1–9.
- (58) Pang, K.-L.; Chin, K.-Y. Emerging Anticancer Potentials of Selenium on Osteosarcoma. *Int. J. Mol. Sci.* **2019**, *20*, 5318.